Flow Turbulence Combust (2011) 87:473–491
DOI 10.1007/s10494-011-9338-z

Large Eddy Simulation of Diesel Fuel Injection and Mixing in a HSDI Engine

Krzysztof Jagus · Xi Jiang

Received: 28 February 2010 / Accepted: 16 February 2011 / Published online: 10 March 2011

Abstract The paper aims to assess the performance of large eddy simulation (LES) in predicting the unsteady reacting flows in internal combustion engines. The incompatibility due to the turbulence dissipation was avoided in the *k*-equation LES formulation. Two versions of the LES have been tested with different filtering. The cell-specific filtering was found to give realistic prediction of the instantaneous temperature and pressure field during the combustion process. The coupling of combustion heat release, temperature field and turbulent flow field was found to be strong in the LES predicted flow and combustion fields which showed wrinkled flame structures. The formulation gives improved agreement with available experimental data.

Keywords Large eddy simulation · Diesel · Injection · Mixing

1 Introduction

Recent advances in computer power and developments in numerical modelling techniques have made it possible for more accurate and detailed investigations of the flow and combustion processes encountered in internal combustion (IC) engines. Difficulties associated with the modelling of in-cylinder flows are well known to both the IC engines and the computational fluid dynamics (CFD) communities. For the modelling and simulations of IC engine flows, the most challenging aspects are associated with high unsteadiness, complex two-phase flows, very broad spectrum of turbulent time and length scales, in addition to the difficulties associated with the

K. Jagus
D-Site SIND-66, Rolls-Royce Plc, Sinfin Lane, Derby DE24 9GJ, UK

X. Jiang (✉)
Engineering Department, Lancaster University, Lancaster LA1 4YR, UK
e-mail: X.Jiang@lancaster.ac.uk

combustion modelling. Careful treatment of these is necessary in order to accurately simulate the process of fuel/air mixing in the cylinder that controls the combustion and emissions.

Recently, Jagus et al. [1] performed a feasibility study of large eddy simulation (LES) in modelling the unsteady fuel injection and mixing in a high-speed direct-injection (HSDI) non-reacting diesel engine environment. Encouraging results were obtained with LES formulation predicting the liquid and vapour fuel concentrations in a much more realistic manner, compared with the results from the traditional CFD based on Reynolds-averaged Navier–Stokes (RANS) modelling approach. For practical IC engine applications, it is necessary to extend the work for reacting flows. LES of combustion has gained much interest in the last few decades. For reacting flows, the modelling of the additional terms arising from the production and destruction of chemical species are challenging even for the traditional RANS approach. LES adds to the complexity further because of the presence of sub-grid quantities and the unsteadiness. Since combustion occurs at the molecular scales, only the finest scales of turbulence have direct influence on the reaction rate. This implies that the interaction of molecular diffusion, reaction rate and turbulent stirring occurs somewhere in the inertial range of turbulent flows and even in the viscosity influenced dissipative range. For automotive engines, those scales can be as small as 10^{-3} mm [2]. In addition, the interaction is highly non-linear and accordingly the development of reliable models is a difficult task. Phenomena like flame-generated turbulence, flame instability and counter-gradient diffusion should all be taken into consideration. As noted by Pope [3], molecular and viscous dissipation ranges are not resolved by traditional LES; hence, information about the interaction of turbulence and chemical rates is contained within the sub-grid scales. Naturally, the energy containing eddies also influence the flame, especially in the premixed cases where quenching due to the excessive turbulence is possible. Turbulent structures especially those involving flow recirculation are also often used to stabilize flame and anchor the flame to the burner. As a result, chemical and turbulent interactions are present throughout the turbulent spectrum [4].

As sub-grid scale modelling of combustion in IC engines is extremely difficult, this study was concentrated on relatively simple approaches for industrial applications of LES, aiming at improving the ability of capturing the unsteadiness in the reacting flows. The preliminary study was focused on a comparison between RANS and two versions of LES. The differences between the LES cases were limited to the details of the combustion modelling, which were conducted to highlight the issue of realistic turbulent timescale prediction. Two stages of the combustion process in an IC engine were analyzed, including the initial and more developed stage of the fuel injection. Comparison with experimental data has been conducted with respect to space averaged results.

2 Mathematical Formulation and Numerical Approach

In LES, the governing equations are time-dependent and obtained from filtering in space. This allows direct computation of the flow structures larger than the filter width as opposed to RANS, where all the scales are time- or ensemble-averaged and the resulting unclosed terms have to be modelled by means of turbulence models. For

the sub-grid scales in LES, a model has to be introduced but it is expected to perform more consistently than the turbulence model in RANS due to the more uniform characteristics of the small scales which are mainly responsible for the dissipation of the energy. More detailed discussion on sub-grid scale models for large eddy simulations of IC engine flows can be found in the literature, e.g. [5, 6]. In this study, the LES was performed using an extensively modified LES version of the KIVA3v code [7], based on the earlier work of Valentino et al. [8, 9] In addition, changes to the specification of the filter width and combustion model were introduced which will be described subsequently. The set of governing equations solved in the code for the LES is given as follows [10].

$$\frac{\partial \bar{\rho}}{\partial t} + \frac{\partial \bar{\rho}\tilde{u}_j}{\partial x_j} = \bar{\dot{\rho}}^S \tag{1}$$

$$\frac{\partial \bar{\rho}\tilde{u}_i}{\partial t} + \frac{\partial}{\partial x_j}\left(\bar{\rho}\tilde{u}_i\tilde{u}_j - \tilde{\tau}_{ij} + \tau_{ij}^{\mathrm{SGS}}\right) + \frac{\partial \bar{p}}{\partial x_i} = \bar{F}_i^S \tag{2}$$

$$\frac{\partial \bar{\rho}\tilde{e}}{\partial t} + \frac{\partial}{\partial x_j}\left(\bar{\rho}\tilde{u}_j\tilde{e} + \bar{q}_j + h_j^{\mathrm{SGS}}\right) + \bar{p}\frac{\partial \tilde{u}_j}{\partial x_j} - \tilde{\tau}_{ij}\frac{\partial \tilde{u}_i}{\partial x_j} + \Pi^{\mathrm{SGS}} + \Theta^{\mathrm{SGS}} = \bar{\dot{Q}}^C + \bar{\dot{Q}}^S \tag{3}$$

$$\frac{\partial \bar{\rho}\tilde{Y}_m}{\partial t} + \frac{\partial}{\partial x_j}\left(\bar{\rho}\tilde{u}_j\tilde{Y}_m - \bar{\rho}\bar{D}_m\frac{\partial \tilde{Y}_m}{\partial x_j} + \Phi_{j,m}^{\mathrm{SGS}} + \theta_{j,m}^{\mathrm{SGS}}\right) = \bar{\dot{\rho}}_m^C + \bar{\dot{\rho}}_m^S \tag{4}$$

Definitions of the variables used in the equations can be found in the literature [10]. The closure of the residual stress tensor is performed using the k-equation model [11, 12], where the sub-grid stress tensor is given as

$$\tau_{ij}^{\mathrm{SGS}} = -2\bar{\rho}\nu_t\left(\tilde{S}_{ij} - \frac{1}{3}\tilde{S}_{kk}\delta_{ij}\right) + \frac{2}{3}\bar{\rho}k^{\mathrm{SGS}}\delta_{ij} \tag{5}$$

The eddy viscosity is given by $\nu_t = C_v\bar{\Delta}\sqrt{k^{\mathrm{SGS}}}$ using the sub-grid turbulent kinetic energy k^{SGS}, which is provided by solving the following equation

$$\frac{\partial \bar{\rho}k^{\mathrm{SGS}}}{\partial t} + \frac{\partial \bar{\rho}\tilde{u}_j k^{\mathrm{SGS}}}{\partial x_j} = -\tau_{ij}^{\mathrm{SGS}}\frac{\partial \tilde{u}_i}{\partial x_j} - D^{\mathrm{SGS}} + \frac{\partial}{\partial x_j}\left(\frac{\bar{\rho}\nu_t}{\mathrm{Pr}_t}\frac{\partial k^{\mathrm{SGS}}}{\partial x_j}\right) + \dot{W}^S \tag{6}$$

In Eq. 6, the sub-grid energy dissipation rate term D^{SGS} is closed by

$$D^{\mathrm{SGS}} = C_\varepsilon\bar{\rho}\frac{\left(k^{\mathrm{SGS}}\right)^{3/2}}{\bar{\Delta}} \tag{7}$$

The values of C_v and C_ε are chosen to be 0.067 and 0.916 [10, 13]. The last term $\dot{W}^s$ in Eq. 7 is the sub-grid turbulence effects due to spray, which follows the original modelling approach used in the RANS version of the KIVA code [7]. The sub-grid heat flux and species mass flux may be modelled using gradient diffusion assumption [10, 13]. The sub-grid viscous work is set to be equal to the dissipation term D^{SGS} from the $k-$equation model.

The governing equations including the formula for the sub-grid dissipation, contain the value for LES filter width $\bar{\Delta}$. In the original implementation, this value

was specified in an ad hoc manner [8]. This is not optimal since computational cells in IC engines inherently vary in size throughout the domain. As a result, averaging is introduced and the sub-grid turbulent kinetic energy was either under resolved or over resolved for most of the cells. This would subsequently influence sub-grid stresses, sub-grid kinetic energy dissipation and consequently the rate of the combustion process. It was, therefore, necessary to provide a more accurate description of the filter width that would vary in space. A simple formula was employed that takes into account the volume of each cell in the system and adjusts the value of filter width accordingly, given by

$$\Delta = \sqrt[3]{\text{Cell Volume}} \tag{8}$$

The combustion model used is a relatively simple approach based on the spark ignition engine derived model of Abraham et al. [14]. It belongs to the family of models based on eddy dissipation. A fundamental condition that needs to be fulfilled is that the combustion process is either kinetic controlled or turbulent mixing controlled. The basis of this model was presented by Magnussen and Hjertager [15]. The feasibility of the approach is justified by the fact that the fluctuations of the reactants are related to the mean values; therefore, the mixing controlled rate can be expressed by the mean reactant species. The underlying assumption of species conversion is that the change rate of density of the mth species is governed by the following formula [16]

$$\frac{d\rho_m}{dt} = -\frac{\rho_m - \rho_m^*}{\tau_{c,m}} \tag{9}$$

In Eq. 9, ρ_m^* is the local instantaneous thermodynamic equilibrium value of the partial density and $\tau_{c,m}$ the characteristic timescale needed to achieve it [16]. The multiscale model implies that those timescales are different for each of the species, as opposed to the model formulation [17] used in the original code, where only single timescale was calculated for all the species present in the system. The determination of the characteristic timescale is based on two main quantities, namely the laminar scale τ_l and the turbulent scale τ_t:

$$\tau_{c,m} = \tau_l + f\tau_t \tag{10}$$

In Eq. 10, f is a coefficient of the degree of turbulent combustion [16]. The laminar timescale is defined as [16]

$$\tau_l = A\left[C_n H_{2n+2}\right]^{0.75}\left[O_2\right]^{-1.5} e^{-E_a/\mathrm{RT}} \tag{11}$$

The model constant A was set up to be 1.625e-11. The turbulent timescale in the original code [7] was based on the ratio of turbulent kinetic energy and its dissipation. While this was well suited for the k–ε-based RANS where k and ε can be determined by solving separate equations, the application in LES is unrealistic. This is because that turbulence kinetic energy in RANS and sub-grid turbulent kinetic energy in LES are fundamentally different concepts. In addition, in LES there is no equation for the dissipation and consequently the prediction must come from the k-equation. This means that both k and ε are estimated in the same manner. In order to supply more accurate information on the turbulent timescale (known also as an eddy turnover

time), a new formula [18] was introduced in the LES performed in this study, given as

$$\tau_t = \left(\frac{\nu}{\varepsilon}\right)^{0.5} \tag{12}$$

The dissipation in Eq. 12 is equal to

$$\varepsilon = 2\nu_t \bar{S}_{ij}\bar{S}_{ij} \tag{13}$$

In Eq. 13, $\bar{S}_{ij}$ is the resolved rate of strain tensor and ν stands for gas phase viscosity. This definition removes the incompatibility and ensures that the eddy turnover time is predicted in a fashion suitable for LES.

With regard to droplet modelling, two commonly used physical models [19] are employed in this study, with each of them responsible for a different breakup regime. They are the Kelvin–Helmholtz (KH) model [20–22] and Rayleigh–Taylor (RT) model [23, 24]. The computational procedure follows the computational parcel concept for liquid injections from orifices, nozzles, etc. The liquid phase is introduced into the chamber as blobs, i.e., big drops with a radius equal to the orifice size. The breakup of these blobs is thought to be due to the growth of KH instabilities, which occur when there is a shear motion of two fluids flowing alongside each other. The "wave" or KH breakup model has been combined with the so-called RT breakup model, in order to estimate the disintegration of the blobs into secondary droplets. The RT instabilities occur when a low density fluid is supporting a higher density fluid against a force. Close to the injector nozzle where the droplet velocities are high, the KH breakup is usually the governing mechanism, whereas the RT breakup becomes more dominant further downstream. The KH model describing diesel spray atomization is based on the linear stability theory. One of the assumptions of the model is that the initial atomization of the injected liquid and subsequent breakup is indistinguishable in a dense spray. The model considers the instabilities which grow at the liquid-gas interface. Their origin can be traced to a shear motion of two liquid films next to each other. The instability caused then leads to the dispersion equation that contains two main parameters in addition to liquid and gas phase properties. In this way, problem of the disintegration of the intact liquid core in the nozzle is by passed.

3 Numerical Results and Discussion

3.1 Engine test conditions and computational cases

A real Hydra diesel engine available at Delphi Diesel Systems was investigated. A range of instantaneous results have been obtained. To save computational time, a 60° section was simulated with periodic boundary conditions applied on both of the side faces. Table 1 summarises the details of engine configuration used. To maximize the benefit of LES, a relatively dense mesh was used in the simulations, which comprises hexahedral elements. The unsteady RANS simulation was performed on a much coarser mesh, which was tested to be sufficient. Refining the mesh in RANS calculations presented no improvement in the accuracy, so the resolution had reached a grid independent state. Table 2 presents a summary of the computational

Table 1 Engine test conditions

Bore diameter	84.46 [mm]
Stroke	88.95 [mm]
Squish	0.8 [mm]
Displacement	500 [cc]
Compression ratio	18.4
Number if injectors	6
Nozzle hole diameter	0.145 [mm]
Spray cone angle	15 [deg]

cases, where in the "LES_eps" case the filter width used is a constant while in the "LES_eddy" case the filter width is cell specific according to Eq. 8.

In this study, it was found that initial conditions have an appreciable effect on the simulation results at the early stage during the first engine cycle. However, the influence diminishes at the later stage when combustion takes place. Initially, the computational domain contained small residual levels of turbulent kinetic energy. Test simulations showed that the initial level of turbulence does not have an appreciable influence on the simulation results. The flow field is dominated by the fuel injection, piston motion, as well as the swirling motion. In the simulations, the swirl number was defined as the ratio between the angular momentum flux and the axial momentum flux, based on the revolutions per minute of the air flow and the crankshaft.

Figure 1 shows an overview of the computational mesh at around 35° crank angle (CA). The piston motion was accounted for in the simulation; therefore, the number of cells and the physical dimension in the Z direction change throughout the computation. Two sets of instantaneous results have been carefully chosen to investigate the temperature fields with the presence of the fuel throughout the combustion cycle. Due to the possible influence of initial conditions on the flow field in the first engine cycle, the instantaneous results shown were taken from the second engine cycle when the influence of initial conditions has been diminished. Snapshots at 5° and 40° were taken to investigate two different stages of the combustion process. In the results obtained, consistent trends have been observed in the spray structure, flow and mixing pattern, as well as temperature fields in other crank angles, compared with these two crank angles. The ignition occurs at around −3° CA and the

Table 2 Summary of the computational cases

	Case A (RANS)	Case B (LES_eps)	Case C (LES_eddy)
Formulation	RANS	LES	LES
Mesh size	66000	595000	595000
LES filter width	N/A	0.6 [mm]	Cell specific
Turbulence model	k–ε	$k-$equation (subgrid)	$k-$equation (subgrid)
Start of injection	−3.5° CA	−3.5° CA	−3.5° CA
Injection duration	30° CA	30° CA	30° CA
Swirl ratio	2.05	2.05	2.05
Chemistry	Shell ignition model; multiscale combustion model	Shell ignition model; multiscale combustion model	Shell ignition model; modified multiscale combustion

Fig. 1 Mesh overview

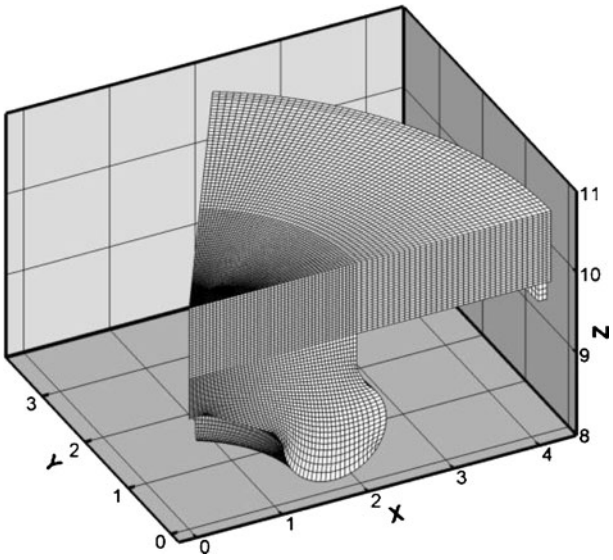

combustion lasts until about 75° so the chosen values should give insight on the initial and a more developed combustion stages.

3.2 Instantaneous results at the initial combustion stage

This section presents comparison of instantaneous results obtained from the unsteady RANS and the two versions of LES. It needs to be noted that the term "instantaneous" is different when applied to RANS or LES. The RANS results presented here are taken from an unsteady simulation for the same instants as the LES results, but the RANS results are not truly instantaneous due to the intrinsic averaging in the methodology. This means that they effectively show state of the flow at the given time with unsteady structures smeared out. This is an important distinction. An unsteady RANS simulation still gives intrinsically averaged results, while LES is able to provide truly time-dependent flow fields. This ability of LES to gain flow unsteadiness is shown in this section and is compared with what is possible using traditional RANS. The ability of the LES code to predict averaged values is demonstrated in Section 3.4, where averaged results are compared between the numerical simulations and experimental data.

Figure 2 indicates the location of the contour plane that has been used for the analysis of the fuel concentrations obtained from the three computational cases summarized in Table 2. The plane inclination is dictated by the angle of the fuel spray and does not intersect the whole cylinder area. Figure 3 presents the contour plots of the fuel vapour mass fraction, along with three-dimensional particle positions at 5° CA projected onto the 2D slice plane, and the corresponding temperature fields.

In Fig. 3, it is evident that the LES results show very different prediction of flow structures compared with the RANS case, in both the liquid and gas/vapour phases. The swirl in the combustion chamber has a high value of 2.05. This means that the pattern of the injected fuel will be affected by the ambient medium. The strong swirl

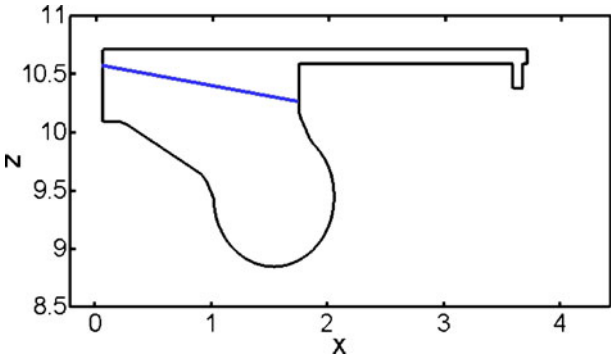

Fig. 2 Contour plane location for 5° CA analysis (units in centimetres)

dominates the trajectory of injected particles, which is also affected by the turbulent flow field associated with the piston motion and fuel injection. Initial conditions do not have a significant impact on the spray pattern because of the strong swirl and piston movement. When comparing Fig. 3a with b and c, it can be seen that the LES predicted fuel vapour mass fraction is much more wrinkled and influenced by the presence of turbulent eddies. The liquid particles are present throughout the domain and are not limited to the vicinity of the core of the jet as they are in the case of RANS. The contours of vapour are much less artificially diffused in the LES_eps and LES_eddy cases. The over-dissipative nature of the k–ε model is responsible for the excessive radial spreading and the unrealistically low penetration of the injected fuel towards the cylinder walls.

The ability to accurately predict fuel/air mixing is very important in terms of the accumulated heat release analysis of IC engines. The penetration of the fuel spray has a profound influence on the rate of heat release, and because of this, LES is expected to provide better agreement with experimental data. More significant particle dispersion in LES cases enhances further the breakup and evaporation process which affects the combustion process. Analysis of the temperature field should provide an indication on quality of the combustion modelling and further highlight differences between the RANS and LES formulations. In Fig. 3, the RANS temperature field is very dissipated. While the low temperature region where the spray is present is predicted reasonably, the outer regions where the burning is initiating appear to be smeared and do not show any wrinkled temperature field which is believed not realistic as combustion in an HSDI engine is highly transient and does not have such a uniform character. The LES cases present temperature field that is much more influenced by the turbulence generated during the expansion stroke. The region where the spray is being injected has much lower temperature than in the RANS case. This is correct since burning does not occur within the liquid jet in the upstream region where there is not enough vapour and spray momentum is high. It is only in the regions where vapour is present that increased temperature values (around 1500 K) can be observed. In the LES_eps case, the temperature in the domain seems to have been under predicted, which was also observed in other planes and other crank angles. There appears to be one region of high temperature in the top corner. LES_eddy case seems to predict the high temperature regions with burning fuels better. Lower region of the domain contains burning zones that are most likely created by the presence of vapour and influenced by the swirl in the

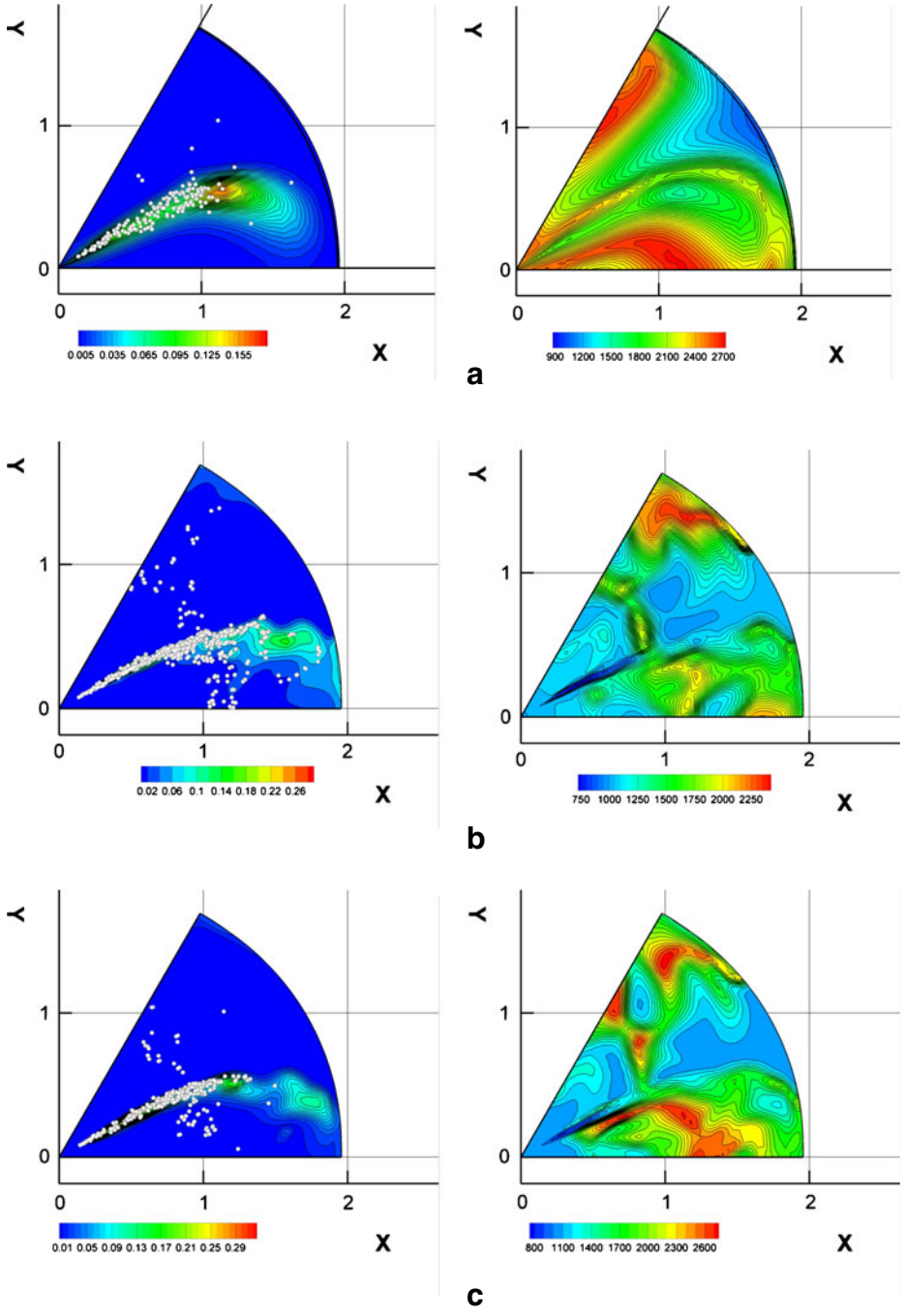

Fig. 3 Vapour mass fractions, 3D particle positions (centimetres) and temperature field (K) at 5° CA: **a** RANS, **b** LES_eps, **c** LES_eddy

cylinder (improved mixing process). The temperature field seems to follow the spray and vapour pattern more closely, although both models predict low temperature region in the middle of the domain, where liquid phase is present. The correlation between fuel presence and temperature is largely absent in the RANS simulation. Overall, the LES predicted temperature fields are much more wrinkled due to the unsteadiness and action of turbulence, something RANS cannot capture.

In the LES_eddy case, the regions of the highest temperature (red colour) seem to exist in the vicinity of the vapour phase (near the jet). This means that fuel is gradually consumed as the liquid evaporates from the jet core and the equivalence ratio is optimal for efficient burning. Interesting feature of the LES_eddy case is the lack of vapour in the upper corner of the periodic domain (it is worth noting that this region is in fact the continuation of the lower portion–periodicity). LES_eps does predict presence of liquid there. This is because the old combustion model (LES_eps) might have under predicted the temperature and the vapour can travel further downstream before being consumed by the flame (again, Fig. 3 needs to be viewed with periodicity in mind, so that the upper portion of the domain is in fact a continuation of the lower bound). In the LES_eddy case, fuel is burnt in the lower region, and this affects the liquid and vapour distribution further downstream. This is evident when looking at the temperature field as there are three regions of high temperature that are most likely responsible for fuel consumption in that area in the new LES_eddy case.

In Fig. 3, for the LES cases, it can be observed from both the temperature and the fuel distribution contours that the flame follows the action of the swirl and, therefore, is influenced by the turbulent flow field, something RANS fails to fully realize in the simulation. The three hot region patches in the LES_eddy case (Fig. 3c) are especially important with the cold one in the middle ($X = 1, Y = 1$). They support the claim that LES is able to capture instantaneous flow structures well [9]. The vortical structures play a significant role in the development and topology of the flame during the combustion process. The coupling between turbulent flow field and heat release, as well as distributions of fuel and temperature seem to be well captured in LES rather than in the RANS. LES with cell-specific filter width seems to perform better than a pre-determined constant filter width.

3.3 Instantaneous results at the advanced combustion stage

When the piston reaches 40° after the top dead centre, the combustion process is in an advanced state and practically all the fuel will have evaporated. Figure 4 shows contours of the temperature. The location of the plane that was used to display the contours of interest is at a constant $Z = 10.1$. This now cuts through the whole cylinder as opposed to the previous intersection of the bowl area only. At 40° CA the combustion process is well developed. Again, there is a strong contrast between RANS and LES results. LES shows much more wrinkled structure and influence of transient turbulent structures that penetrate into high temperature regions and affect the behaviour of the flame. For the differences between the two LES cases, it is noted that there is an unrealistic, almost vertical region of moderate temperature levels at about $X = 2$ captured by LES_eps (Fig. 4b). It looks like a discontinuity and cannot be observed in Fig. 4c. The large patch of high temperature region in Fig. 4b between $X = 1$ and $X = 2$ can also be questionable to certain extent. LES_eddy

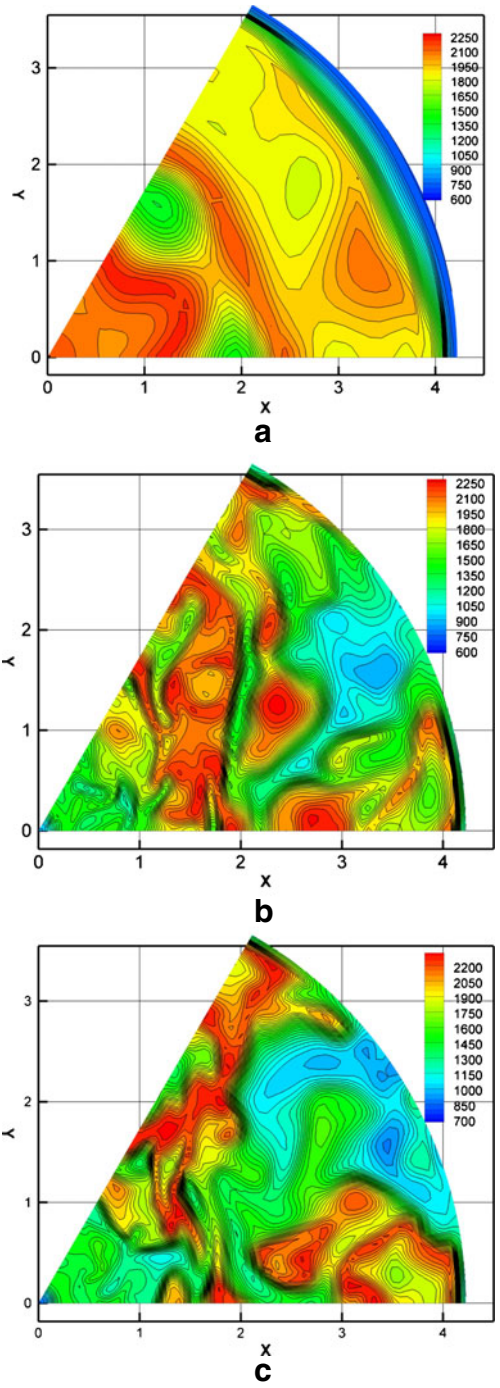

Fig. 4 Temperature contours (K) at 40° CA: **a** RANS, **b** LES_eps, **c** LES_eddy (length in centimetres)

does not predict such a large and uniform region. Instead, much more irregular field is observed in that area. This may be explained by the more realistic prediction of the LES_eddy formulation for the sub-grid scales with dynamically calculated filter

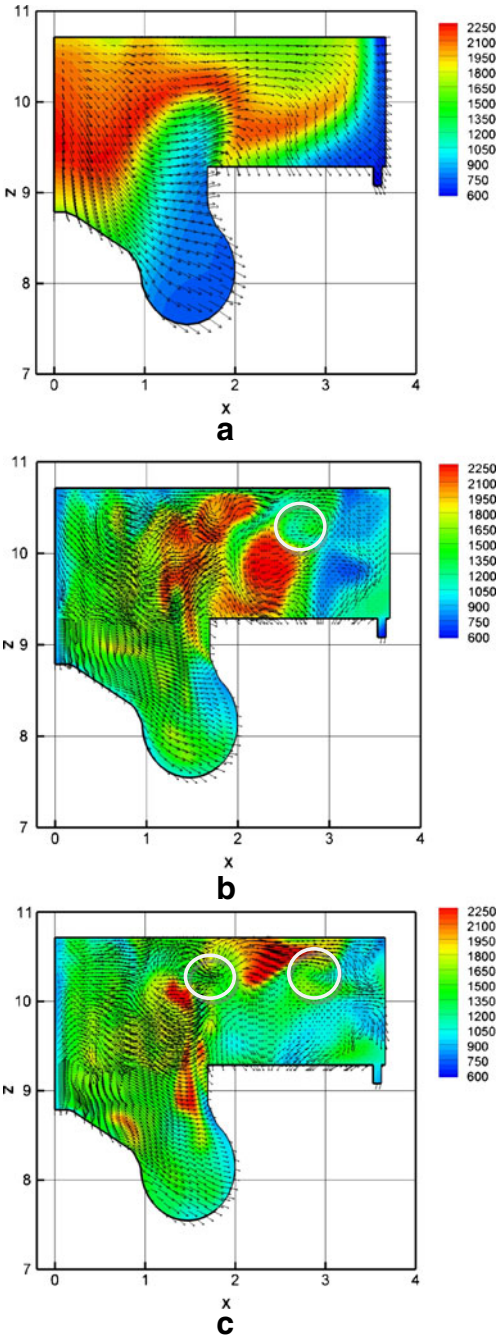

Fig. 5 Side temperature contours (K) and velocity field on a vertical plane: **a** RANS, **b** LES_eps, **c** LES_eddy (length in centimetres)

width. Large temperature and pressure gradients can modify the flow field, leading to significantly different flow and combustion predictions. Examining the regions near the cylinder wall, there are further significant differences between the three cases investigated. Since the walls are cooler than the combusting gas, it would be expected that temperature distribution would to some extent reflect that. Here, the RANS case seems to capture the correct trend while at the same time over predict the influence of cool cylinder walls. It is worth noting that the near-wall temperatures predicted by the LES need to be treated with caution since the law-of-the-wall approach adopted is not suitable for the LES, which was developed for and therefore compatible with the RANS approach.

To further examine the temperature distribution and the influence of turbulent flow field on the quality of combustion, side plots have been constructed on a plane that cuts through the middle of the 60° grid. Those plots are presented in Fig. 5. In addition to the temperature field, visualization of the flow field by means of vectors has been superimposed on the contours. Velocity levels predicted by LES are very high, especially in the region up to $X = 2$. Reasons for this are most likely to be the tumble flow generated by the downstream piston motion and the influence of the bowl area which augments the turbulence generation. The temperature distribution closely follows the velocity field. Examining Fig. 5c at $X = 1.8$ where two high temperature regions exist, it becomes clear how the turbulent vortices are able to influence the temperature distribution and most likely the flame behaviour. In this region, flame might be subject to quenching by the strong flow and that could be the reason for the separation of those two hot regions. In the near-wall region, there is a strong clockwise-rotating vortex, and the relatively low temperatures in that region (around 1000 K) could be explained by the strong convection of the flow and the presence of walls. On the other hand, large temperature gradients in that area (high temperature on one side and cool walls on the other) may generate additional flow motion due to high pressure gradients presented.

A close examination of Fig. 5b revealed a very pronounced vortex at $X = 2.9$ that is visible both when examining the velocity vectors and when analyzing the temperature field in that region. This indicates that the coupling of turbulence and combustion is of a two-way nature in LES. Case C (LES_eddy) captures vortices at $X = 2.8$, $Z = 10.2$ and $X = 1.9$, $Z = 10.2$ that clearly modify the shape of the high temperature front. For clarity, the vortices in question have been highlighted by the white circles.

Examining the bowl area, much higher values are predicted by LES than RANS, which essentially fails to account for presence of hot gases in that region completely. In general, high velocity of the fluid and presence of swirling influences the combustion process. The instantaneous results from LES are vastly different with the RANS results, which are nothing more than averaged flow properties. Efficient mixing prediction by LES allows for realistic fuel burning and combustion heat release in spatially distributed fuel rich regions. Unfortunately, RANS simulation fails to capture those effects. The combustion process is largely decoupled from the motion of the gas phase. The flow field in the RANS case is also much more uniform throughout the cylinder, failing to capture the unsteady vortices.

The interactions of turbulence and temperature distribution can also be visualized by iso-surfaces of the temperature fields. Figure 6 shows the temperature value of 1600 K for all the three cases. Apparently the LES temperature prediction is very different from that by RANS. Figure 6b, c shows a wrinkled field that is a direct

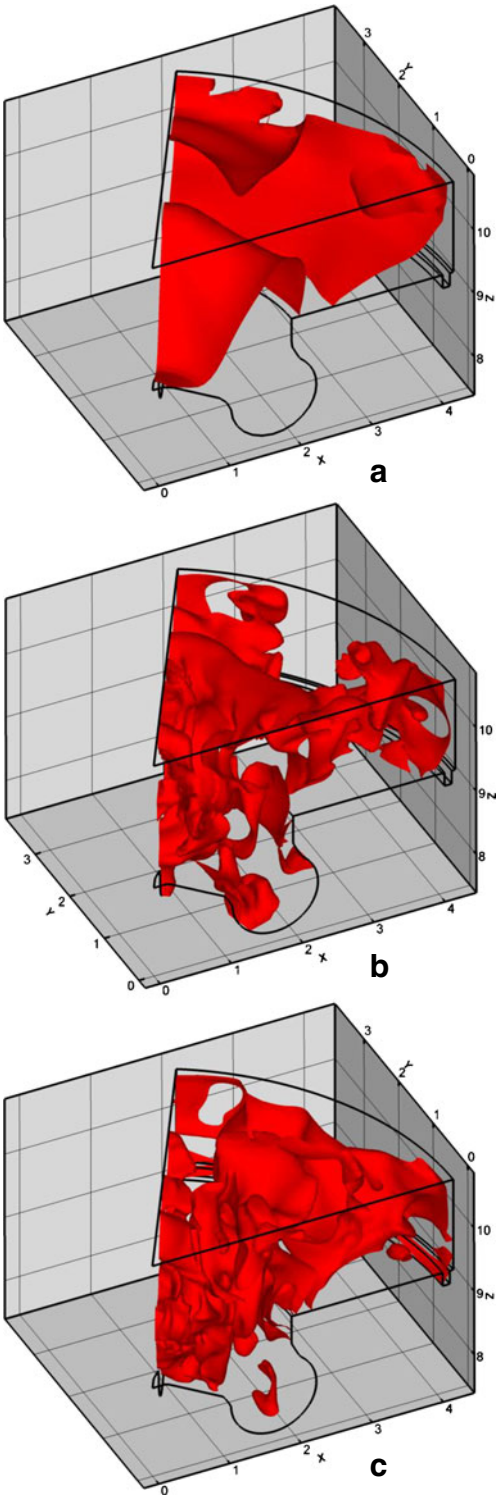

Fig. 6 Iso-surfaces of temperature at 1600 K: **a** RANS, **b** LES_eps, **c** LES_eddy

consequence of unsteady flow structures modifying the temperature field. RANS results are once again characterized by the lack of unsteady features. The turbulence is represented in the mean quantities, but the flow unsteadiness has been inevitably lost.

In IC engine flow and combustion simulations, pressure prediction is very important for comparison with experimental data, which gives a very useful indication on the performance of the model. Figure 7 shows the pressure distribution in the same plane that was used in Fig. 5. The unit for pressure is provided in dynes per square centimetre. The unit range is presented in an individual manner, meaning that each of the cases has its own respective range. There are notable differences not only between RANS and LES but between performances of the two LES formulations.

The pressure prediction is significantly different for all three cases and this is where the LES_eddy case may prove to be more realistic than the other two cases. The distribution of pressure values in Fig. 7c seems realistic and follows the temperature distribution. Examining Fig. 5c, it can be observed that high temperature regions correspond exactly to the pressure values in the domain (Fig. 7c). The area with the centre at around $X = 1.7$ and $Z = 10.3$ can be distinguished in both figures. The unsatisfactory performance of RANS is augmented by the fact that the pressure values are significantly underpredicted, which was evident when compared with experimental data (such as the one indicated in Fig. 8). LES_eps gives better quantitative results but the distribution is largely decoupled from the temperature field. The RANS and LES_eps show regular vertical "segmentation" of the pressure contours, which may be related to the swirling motion in the chamber but it can still be questionable in the near-wall region at the far end (right-hand side of the figures shown) since the flow is highly three-dimensional and turbulent. It is clear that the prediction of pressure is more realistic with the LES_eddy model with smaller gradients and in general more uniform distribution, reflecting the distributions of both the temperature and the flow fields.

In all three cases, there are small artefacts visible on the left-hand side of the plane (near the axis of the three dimensional cylinder). Their presence can be explained by the relatively high distortion of the computational cells in the near-axis area, where the aspect ratio of the computational cell is inevitably compromised. Other construction of mesh was not possible due to the limitations of the KIVA code [7] associated with the face connectivity procedures. Influence of those artefacts on the results is believed to be insignificant since there is no appreciable flow change in the nearby region.

3.4 Comparison with experimental data

By comparing the computational results with the in-house experimental data available at Delphi Diesel Systems, this subsection further assesses the performance of RANS and the two LES formulations when predicting space averaged results. In the LES performed, the small cycle variation was caused by the differences in initial/starting conditions of different cycles, which is not significant. The spatial average of the results was carried out for the second engine cycle when the influence of initial conditions had been diminished. Experimental data were available for comparison and served as a benchmark. Figure 8 shows the curve of accumulated heat release with respect to the crank angle. The performance of LES models is

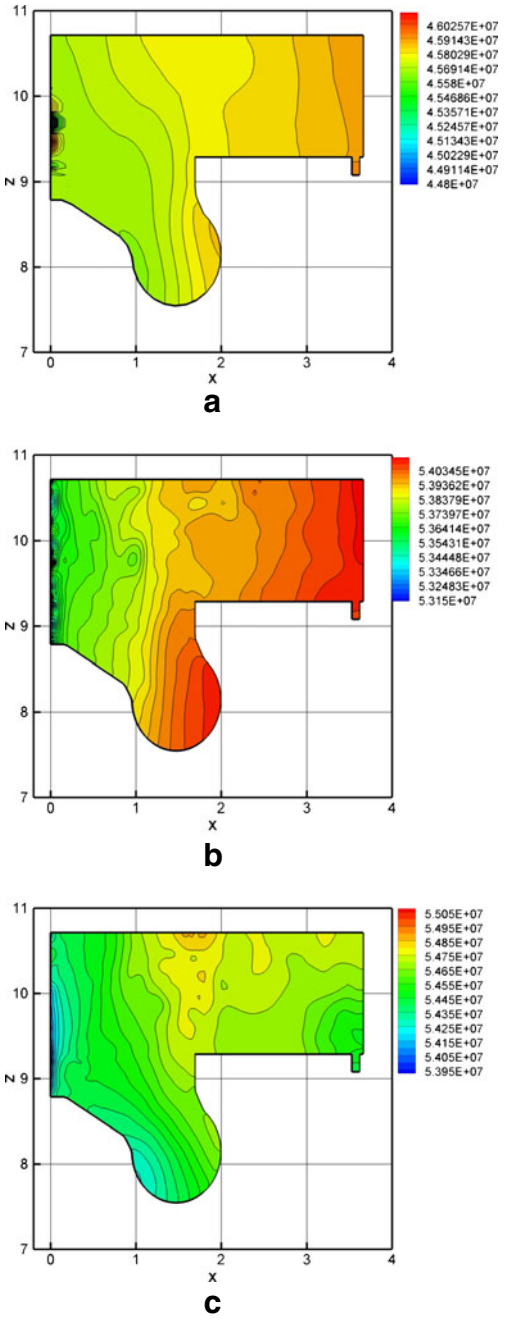

Fig. 7 Pressure distribution (dynes/square centimetre) on a vertical plane: **a** RANS, **b** LES_eps, **c** LES_eddy (length in centimetres)

in good agreement with the experiment, both qualitatively and quantitatively. The LES_eddy gives a very slight over prediction between 20° and 60°. For other crank angle values, the agreement is highly satisfactory. RANS values severely under-

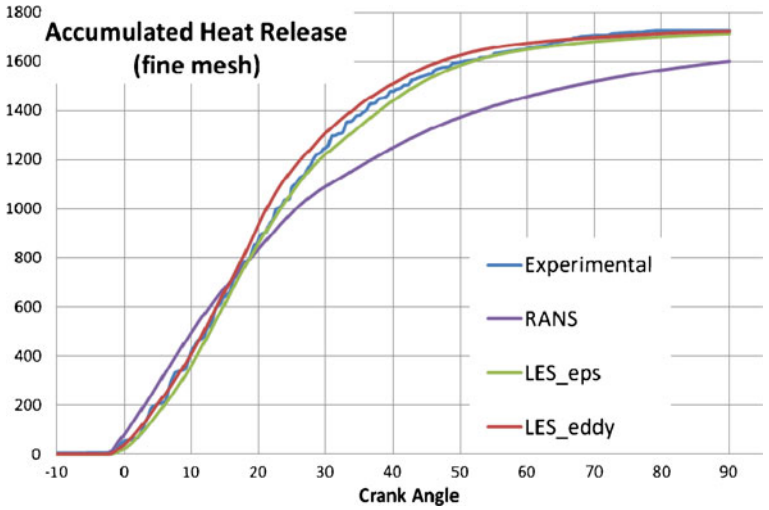

Fig. 8 Comparison of the accumulated heat release rate (unit: Joule)

predicted the experimental data after 20° and over-predicted for earlier crank angle values. The shape of the curve least resembles the data from the experiment.

When analyzing the accumulated heat release, it is important for the model to correctly predict the stabilization of the values after the process of combustion is completed. RANS again fails to capture the correct trend. At the same time, LES_eddy does reach the quasi-steady state in accordance with experimental data. LES_eps case also has a good performance, although the steady state reaches slightly lower value than the one predicted by LES_eddy and the experiment. Overall, the ability of LES_eddy case to predict the accumulated heat release (and accordingly the pressure) in engine cylinder throughout the cycle is superior to the RANS results. There are marked improvements over the original RANS formulation, both in terms of absolute values and the shape of the accumulated heat release versus crank angle curve.

4 Concluding Remarks

Flows in HSDI engines are amongst the most difficult to model numerically. High unsteadiness, two-phase flow, self-ignition, combustion, wall treatment all call for advanced physical models to obtain realistic numerical results. Up until recently, RANS was a common approach to model engine flows. However, its capability in predicting complex unsteady engine flows is seriously limited by its inability in modelling complex unsteady flow fields and vortical structures.

This work aimed to describe the developments of the application of LES to multiphase, reacting flows. Some encouraging results have been obtained and significant improvements over RANS version of the KIVA have been achieved in the preliminary investigation. Two versions of the LES code have been tested with differences in filtering. The incompatibility due to the turbulence dissipation was avoided in the LES formulation. The new formulation was found to give more realistic prediction

of the instantaneous temperature and pressure field during the combustion process. The coupling of combustion heat release, temperature field and turbulent flow field was found to be very strong, a feature that was absent in the reference RANS results. In LES, unsteady flow features are responsible for the dynamic temperature field. LES predicts much more wrinkled flame structures, where the vortices can augment or suppress the reaction depending on the local vorticity. This analysis of unsteady features is not possible using the RANS method, where information about time dependent flow structures is largely lost. Finally, comparison with experimental data has been conducted where numerically generated results have been assessed against the accumulated heat release plots from experiments. LES and RANS cases confirmed the improved performance of LES in terms of both quantitative and qualitative agreement. The updated version of the LES gave a very good agreement with the experimental data. This can be attributed to the better representation of mixing, which is crucial for the correct prediction of accumulated heat release rates and in-cylinder pressure of combustion engines.

Acknowledgements The computational work was supported by the UK Consortium on Computational Combustion for Engineering Applications (COCCFEA) under EPSRC Grant No. EP/D080223/1 and Delphi Diesel Systems. The authors would like to thank Drs. Gavin Dober, Godfrey Greeves and Nebojsa Milanovic of Delphi for his financial support and valuable discussions on the results.

References

1. Jagus, K., Jiang, X., Dober, G., Greeves, G., Milanovic, N., Zhao, H.: Assessment of large-eddy simulation feasibility in modelling the unsteady diesel fuel injection and mixing in a high-speed direct-injection engine. Proc. IMechE Part D: J. Automobile Engineering **223**, 1033–1048 (2009)
2. Lumley, J.L.: Engines: An Introduction. Cambridge University Press, Cambridge (1999)
3. Pope, S.B.: Turbulent Flows. Cambridge University Press, Cambridge (2008)
4. Bray, K.N.C.: The challenge of turbulent combustion. Proc. Combust. Inst. **26**, 1–26 (1996)
5. Pomraning, E.: Development of Large-Eddy Simulation Turbulence Models. PhD Thesis. University of Wisconsin-Madison, Madison (2000)
6. Celik, I., Yavuz, I., Smirnov, A.: Large eddy simulations of in-cylinder turbulence for internal combustion engines: a review. Int. J. Engine Res. **2**, 119–148 (2001)
7. Amsden, A.: KIVA-3V: a block-structured KIVA program with block-structured mesh for complex geometries. Report LA-13313_MS, UC-1412. Los Alamos National Laboratory, Los Alamos (1997)
8. Valentino, M.: Numerical Simulations of Transient Gas and Spray Jets Under Diesel Conditions. PhD Thesis. Brunel University, Uxbridge (2006)
9. Valentino, M., Jiang, X., Zhao, H.: A comparative RANS/LES study of transient gas jets and sprays under diesel conditions. Atomization Sprays **17**, 451–472 (2007)
10. Sone, K., Menon, S.: The effect of subgrid modeling on the in-cylinder unsteady mixing process in a direct injection engine. ASME J. Eng. Gas Turbine Power **125**, 435–443 (2003)
11. Menon, S., Calhoon, W.: Subgrid mixing and molecular transport modelling for large-eddy simulations of turbulent reacting flows. Proc. Combust. Inst. **26**, 59–66 (1996)
12. Menon, S., Yeung, P., Kim, W.: Effect of subgrid models on the computed interscale energy transfer in isotropic turbulence. Comput. Fluids **25**, 165–180 (1996)
13. Sone, K., Patel, N., Menon, S.: KIVALES: Large Eddy Simulations of Internal Combustion Engines. Part I: Theory and Formulation. Technical report CCL-2001–008. Georgia Institute of Technology, Atlanta (2001)
14. Abraham, J., Bracco, F.V., Reitz, R.D.: Comparisons of computed and measured premixed charge engine combustion. Combust Flame **60**, 309–322 (1985)
15. Magnussen, B.F., Hjertager, B.H.: On mathematical modelling of turbulent combustion with special emphasis on soot formation and combustion. Proc. Combust. Inst. **16**, 719–729 (1976)

16. Xin, J., Montgomery, D., Han, Z., Reitz, R.D.: Multidimensional modeling of combustion for a six-mode emissions test cycle on a DI diesel engine. ASME J. Eng. Gas Turbine Power **119**, 683–691 (1997)
17. Reitz, R.D., Bracco, F.V.: Global kinetics models and lack of thermodynamic equilibrium. Combust. Flame **53**, 141–143 (1983)
18. Yaga, M., Endo, H., Yamamoto, T., Aoki, H., Miura, T.: Modeling of eddy characteristic time in LES for calculating turbulent diffusion flame. Int. J. Heat Mass Transfer **45**, 2343–2349 (2002)
19. Jiang, X., Siamas, G.A., Jagus, K., Karayiannis, T.G.: Physical modelling and advanced simulations of gas liquid two-phase jet flows in atomization and sprays. Prog. Energy Combust. Sci. **36**, 131–167 (2010)
20. Reitz, R.D.: Modeling atomization processes in high-pressure vaporizing sprays. At. Spray Technol. **3**, 309–337 (1987)
21. Chigier, N., Reitz, R.D.: Regimes of jet breakup and breakup mechanisms (physical aspects). In: Kuo, K.K. (ed.) Recent Advances in Spray Combustion: Spray Atomization and Drop Burning Phenomena, vol. 1, pp. 109–135. AIAA, Reston (1996)
22. Lin, S.P., Reitz, R.D.: Drop and spray formation from a liquid jet. Annu. Rev. Fluid Mech. **30**, 85–105 (1998)
23. Reitz, R., Diwakar, R.: Effect of Drop Breakup on Fuel Sprays. Society of Automotive Engineers Technical Paper 860469 (1986)
24. Su, T.F., Patterson, M.A., Reitz, R.D., Farrell, P.V.: Experimental and numerical studies of high pressure multiple injection sprays. SAE Paper 960861 (1996)